PHYSICAL REVIEW B **86**, 195314 (2012)

Induced currents in the quantum Hall regime: Energy storage, persistence, and *I*-*V* characteristics

M. J. Smith, A. Usher, C. D. H. Williams, and A. Shytov
School of Physics, University of Exeter, Stocker Road, Exeter EX4 4QL, UK

A. S. Sachrajda, A. Kam, and Z. R. Wasilewski
Institute for Microstructural Sciences, National Research Council of Canada, Ottawa, Ontario, Canada K1A 0R6
(Received 20 June 2012; revised manuscript received 9 November 2012; published 26 November 2012)

Induced currents associated with the quantum Hall effect are studied in the temperature range 39 mK to 1.6 K, and at Landau-level filling factors $\nu = 1,2,3,4$, and 6, using torsion-balance magnetometry. A quantitative link is demonstrated between (nonlinear induced current) vs (inducing electromotive force) curves, and the subexponential decay of the induced current in a static magnetic field. The energy storage in the induced currents is reexamined with the conclusion that the predominant mechanism for storage is inductive, through the mutual inductance between the sample and the magnet, not capacitive as previous reports have assumed. The temperature dependencies of the currents are consistent with previous models, except for a low-temperature saturation at filling factors $\nu = 1$ and $\nu = 2$, which we attribute to electron heating.

DOI: 10.1103/PhysRevB.86.195314 PACS number(s): 73.43.Fj, 73.23.Ra, 73.43.Qt

I. INTRODUCTION

Studies of induced currents in the quantum Hall effect (QHE) regime have greatly improved our understanding of the quantum-fluid states underlying the effect (for a review, see Usher and Elliott[1]). Following the first observations of induced currents in pioneering magnetometry experiments,[2,3] induced currents have been used to study the breakdown of the QHE at high current densities,[4–9] and, through measurements of their decay in static magnetic fields using various techniques,[10–15] to infer a value of longitudinal resistivity smaller than in any other nonsuperconducting system. Despite being 1000 times larger than the currents used in conventional transport measurements, induced currents have no observable effect on such measurements. It has been speculated[11] that induced currents flow in the compressible strip at the outside edge of the innermost incompressible strip present in the two-dimensional electron system (2DES) at integer Landau-level filling factors,[16] which would explain their isolation from the edge-state currents detected in conventional transport measurements. In this paper we demonstrate a quantitative link between the nonlinear induced current versus inducing electromotive force (I-V) characteristic of the induced currents and their decay. We further identify a previously overlooked mechanism for the energy storage associated with induced currents, namely the mutual inductance between the circulating current and the externally applied magnetic field. We compare this with other energy storage mechanisms (self-inductance and capacitance) and show that the mutual inductance term dominates these other contributions.The magnitude of the saturation current of the I-V characteristic in our sample is shown to be determined by electron self-heating, rather than by quantum Hall breakdown.

II. EXPERIMENT DETAILS

The experiments were performed on a two-dimensional electron system (2DES) within a GaAs/(Al,Ga)As heterojunction of area 4.0 mm × 4.5 mm, grown at the Institute for Microstructural Sciences.[17] The carrier concentration of the 2DES was 2.01×10^{15} m^{-2} and its mobility was 103 m^2 V^{-1} s^{-1} at 4.2 K, determined from the period of its Shubnikov–de Haas oscillations. The sample was mounted on the rotor of a differential torsion-balance magnetometer[18] with the normal to the 2DES at an angle of $\theta = 20^\circ$ to the applied magnetic field (see inset to Fig. 1). The magnetometer was calibrated at base temperature by applying a DC voltage between the capacitance electrode on the rotor and one of the fixed capacitor plates. The resulting electrostatic force produces a torque that can be calculated from the capacitor geometry and this can be used to determine the conversion factor between change in capacitance and magnetic moment. Comparison with other calibration methods that can be carried out only at room temperature (for instance placing a known mass at a known position on the rotor) demonstrates that this method provides a calibration with an uncertainty of about 10%.

The sample under investigation had a metallic split gate defined on the surface, 110 nm above the 2DES. This was used in other experiments to produce a quantum point contact but its presence is not relevant to the results presented in this paper.

The magnetometer was placed in the mixing chamber of a dilution refrigerator (Oxford Instruments Kelvinox AST200) and measurements were made between 39 mK and 1.6 K. The dilution refrigerator was operated in single-shot mode to eliminate vibrational noise. The magnetic field was produced by a 19 T superconducting solenoid, driven by an Oxford Instruments IPS 120-20 digital power supply.

III. RESULTS

A. Sweep-rate *I*-*V* characteristics

Figure 1 shows the magnetometer torque as the magnetic field is swept at 1.6 mT s^{-1}, at a temperature of 40 mK. The features that reverse direction when the sweep direction is reversed are caused by QHE induced currents. An I-V curve for the induced currents can be constructed from raw data such as that of Fig. 1 because the magnetic moment is

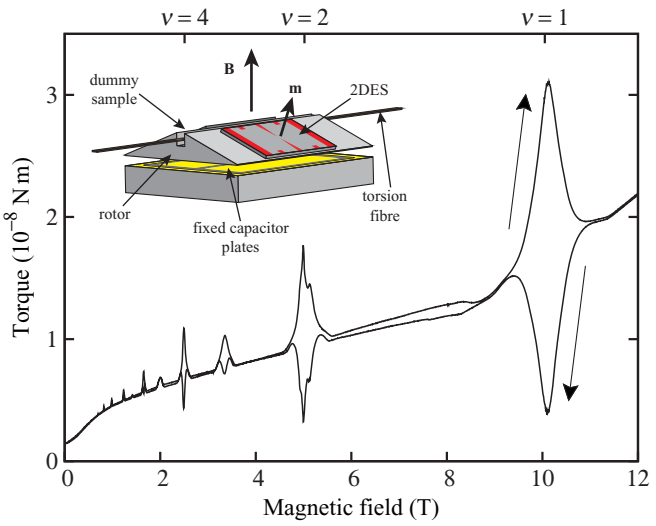

FIG. 1. (Color online) Typical magnetometer output of torque vs magnetic field at a temperature of 40 mK and a magnetic-field sweep rate of 1.6 mT s^{-1}. The arrows indicate the sweep directions. QHE induced currents are observed at Landau-level filling factors $\nu = 1,2,3,4$, and 6. The other, nonreversing features are caused by capacitive coupling between the magnetometer and the 2DES. The inset is a schematic diagram of the torsion-balance magnetometer. The magnetic moment **m** of the 2DES produces a torque $\mathbf{m} \times \mathbf{B}$, which is detected as an imbalance of the differential capacitor formed by an electrode on the underside of the rotor and the two fixed capacitor plates.

proportional to the circulating current which is induced by an electromotive force proportional to the magnetic-field sweep rate. The magnitude of the magnetic moment, m, of a loop carrying a current I is

$$m = IA, \tag{1}$$

where A is the 2DES area and it is assumed that the current flows around the perimeter of the sample. The electromotive force ε is given by

$$\varepsilon = -\frac{d\Phi}{dt} = -A\cos\theta\frac{dB}{dt}, \tag{2}$$

where Φ is the magnetic flux and B is the magnitude of the magnetic induction.

For each sweep rate, an up- and a down-sweep were measured, and the induced current was determined from the peak-to-trough height. Figure 2 presents the I-V curves, over a range of temperatures from 100 mK to 1600 mK, for Landau-level filling factors $\nu = 1,2,4$, and 6. All the I-V curves are nonlinear with the induced currents rising rapidly with electromotive force and saturating at tens of nanovolts, corresponding to sweep rates of $\sim$2 mT s^{-1}. The saturation values of the induced currents tend to be reduced as the temperature is increased. It is notable that for $\nu = 1$ and $\nu = 2$, the induced currents are already saturated even at the lowest sweep rates. The current induced at $\nu = 2$ was the least sensitive to temperature and was still detectable at 1600 mK. At low temperatures the induced currents at filling factors $\nu = 1,2$, and 4 all saturate at the same critical current of 0.28 ± 0.02 mA.

At $\nu = 4$ and $\nu = 6$ a detailed examination was carried out of the low-electromotive-force portion of the I-V curve, which involved sweeping the magnetic field at the minimum rate (16 μT s^{-1}) that the digital power supply allowed before digitization steps became apparent. The remarkable result is that the I-V curve remains nonlinear to the lowest electromotive force attainable (0.27 nV) implying that the resistivity continues to decrease with current, never reaching an observable limit.

We were able to examine the behavior at low electromotive force for $\nu = 4$ and 6, but not for $\nu = 1$ and 2 because of the extremely slow sweep rates involved and the relatively wide magnetic field range of the $\nu = 1$ and $\nu = 2$ induced currents. The run time of the experiments was limited by the need to operate the dilution refrigerator in single-shot mode to minimize vibrational noise caused by changeover of the dilution-refrigerator sorption pumps.

B. Temperature dependence

Figure 3 shows the temperature dependence of the induced current at $\nu = 1$ for the temperature range 39 mK to 800 mK. At temperatures up to 400 mK the most significant change is a decrease in peak width with increasing temperature. There is also a slight increase in peak height which is not understood but is close the level of the experimental uncertainty (10%). Above 400 mK both the peak height and the width fall. Figure 4 shows the temperature dependencies of the induced current peak heights for filling factors $\nu = 1,2,3,4$, and 6. The $\nu = 1$ and 2 (and possibly 4) induced currents saturate at low T to a common value. The induced currents at the other filling factors never reach this value and therefore do not saturate. Note that these data were acquired in a separate experiment to those of Fig. 2, but the values of induced currents under comparable conditions are consistent to within 10%.

C. Decay measurements

Because of the extremely low dissipation in the quantum Hall regime, induced currents are found to be long lived after the magnetic field is swept and then halted at integer filling factor. In order to study the decay of induced currents it is important first to establish the magnetometer zero offset. This is done by the process described in Fig. 5. Three examples of the decay of the induced currents are shown in Fig. 6. At all three filling factors shown there is a rapid initial decay followed by a slower one. For filling factors $\nu = 1$ and 2, the slower decays have the form of a power law, consistent with previous reports that the decay is not exponential.[15] However, for $\nu = 4$ the longer decay appears to be exponential and reduces the current to zero. Decays become difficult to measure for higher filling factors because they become fast enough to be masked by transient effects when the magnet stops sweeping. We note that the induced current at $\nu = 1$ decays more slowly than the one at $\nu = 2$. This result is unexpected because the separation between the highest full and the lowest empty Landau level is smaller for $\nu = 1$ because the levels are spin split. This will be discussed below. In Sec. IV B a quantitative link is made between the decays of induced currents and their I-V characteristics.

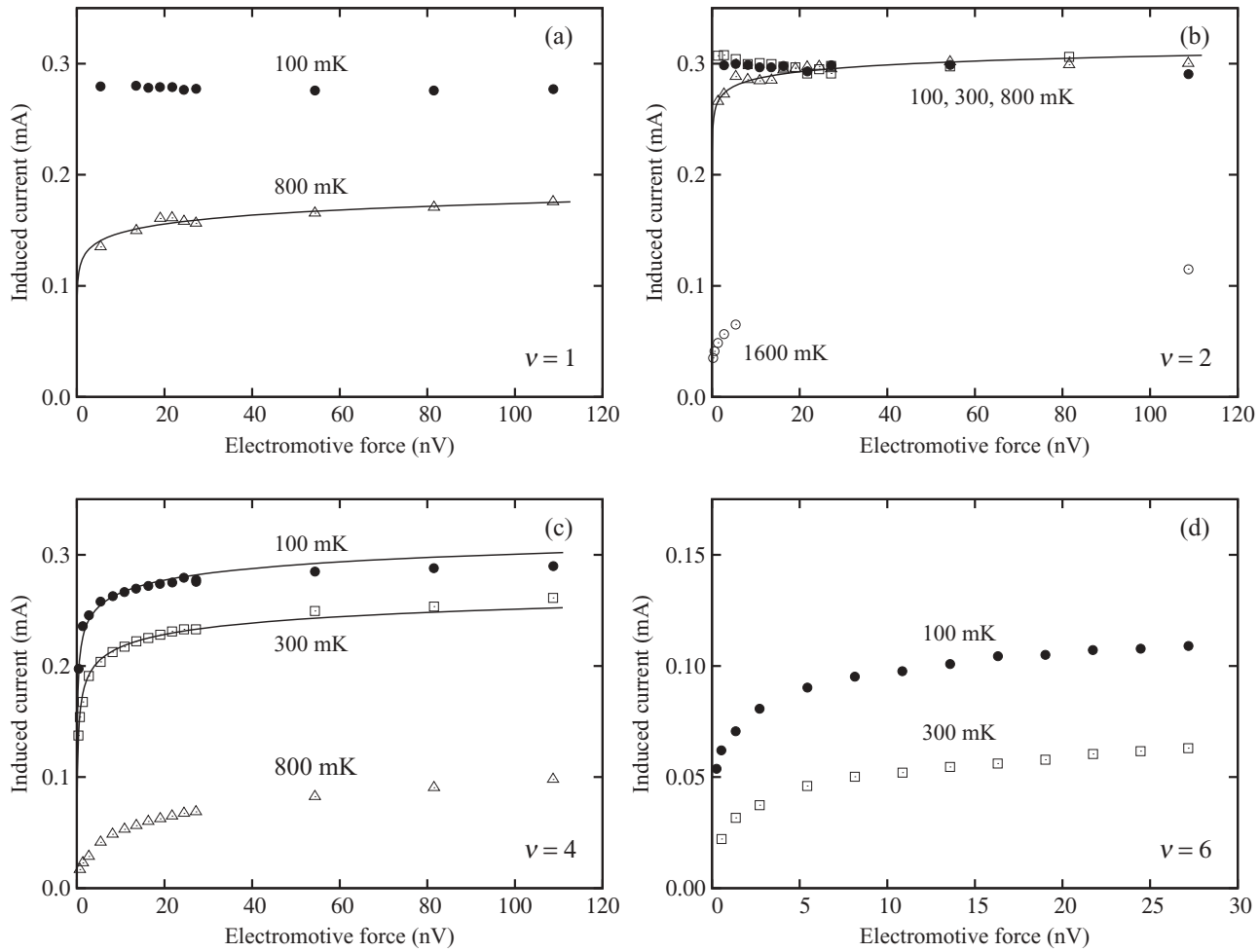

FIG. 2. Nonlinear I-V curves for $\nu = 1$ (a), $\nu = 2$ (b), $\nu = 4$ (c), $\nu = 6$ (d), at various temperatures: 100 mK, filled circles; 300 mK, open squares; 800 mK, open triangles; 1600 mK, open circles. The magnetic-field sweep rate has been converted to electromotive force and the magnetic moment to current, as described in the text. At high electromotive force, the current saturates. The solid lines following the 800 mK data for $\nu = 1$ in (a), the 800 mK data for $\nu = 2$ in (b), and the 100 and 300 mK data for $\nu = 4$ in (c) are empirical fits used to relate I-V curves to induced-current decays, as discussed in Sec. IV B.

IV. DISCUSSION

A. Energy storage and dissipation

Previous investigations of induced current decays have suggested that the energy associated with the induced current is primarily stored "capacitively" in the Hall electric field, and that this energy decays through a resistance proportional to $1/\sigma_{xx}$ (for reasons discussed below).[3,10] Jones *et al.*[10] also considered the self-inductance of the induced current but concluded that it made a negligible contribution to energy storage. A simple qualitative argument supports this conclusion: The inductance and capacitance of a circular 2DES of radius r are given approximately by $L \approx \mu_0 r$ and $C \approx \epsilon_0 \epsilon_r r$. The ratio of the inductive to the capacitive energy is then LI^2/CV_r^2, where I is the induced current and V_r is the radial voltage due to the Hall effect associated with the induced current. Since

$$V_r = \rho_{xy} I \tag{3}$$

(where ρ_{xy} is the quantized Hall resistivity, and we have neglected any radial current), this ratio becomes $\mu_0/\epsilon_0\epsilon_r\rho_{xy}^2$, 2.6×10^{-4} for a 2DES in GaAs, at $\nu = 4$, which is in order-of-magnitude agreement with the calculations of Jones *et al.*[10]

However, these previous studies did not discuss the mutual inductance between the induced current and the solenoid producing the magnetic field. Table I summarizes the contributions to the energy associated with the induced current. Details of how these are calculated are given in the Appendix. We see from the table that the mutual inductance term is 3.5 orders of magnitude larger than the capacitive estimate, and 6.5 orders of magnitude greater than the self-inductance term.

The charging and discharging of the electromagnetic energy associated with an induced current can therefore be modeled by the differential equation

$$L_s \frac{dI}{dt} + RI + \frac{Q}{C} = M \frac{dI_m}{dt}, \tag{4}$$

where Q is the charge accumulated on the capacitance C (described in more detail in the Appendix), and R is the relaxation resistance, the effective resistance resulting from residual dissipation in the sample. We have shown that the first

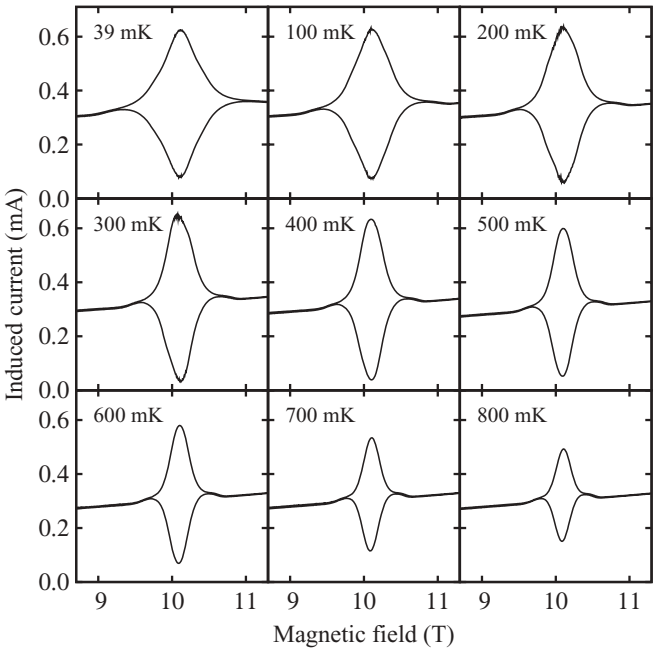

FIG. 3. Temperature dependence of the induced current at $\nu = 1$. The induced currents are inferred from measurements of torque such as those shown in Fig. 1.

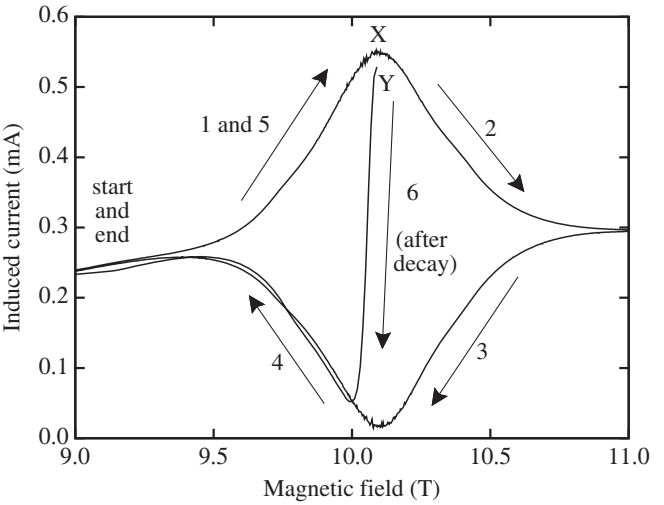

FIG. 5. Establishing the magnetometer zero offset for the induced-current decay at $\nu = 1$, 100 mK. Starting at 9 T the magnetic field is swept through the $\nu = 1$ feature to 11 T (arrows 1 and 2) and back down to 9 T again (arrows 3 and 4). The zero offset is the average of these two curves. The decay is then initiated by sweeping up to $\nu = 1$ (10.09 T, point X). After the decay (Y) the magnetic field is swept down to 9 T to confirm that no drift occurred during the decay. In this decay (shown in Fig. 6) the induced current is reduced by about 10% in 35 000 s.

term in this equation is always negligible. While the magnet is sweeping, energy is being stored both in the capacitance and in the mutual inductance. When the magnet stops sweeping, the mechanism by which the energy stored in the mutual inductance is discharged depends on the operation of the magnet power supply. The decaying sample current will induce an electromotive force across the magnet. Assuming that the magnet power supply acts as a constant current source, it will provide a voltage that exactly cancels this electromotive force and the energy stored in the mutual inductance will be dissipated within the power supply. In this case, the term on the right-hand side of Eq. (4) becomes zero and the decay of the current within the sample can simply be modeled as the discharge of a capacitor through a resistor.

The relationship of R to the sample conductivity can be obtained from the following argument. As the azimuthal induced current decays, the charge built up at the edge of the sample returns to the center producing a radial current, $I_r = 2\pi r j_r = dQ/dt$. Now,

$$j_r = \sigma_{xx} E_r + \sigma_{xy} E_\phi, \tag{5}$$

where E_r and E_ϕ are the radial (Hall) and azimuthal components of the electric field, respectively. During the decay,

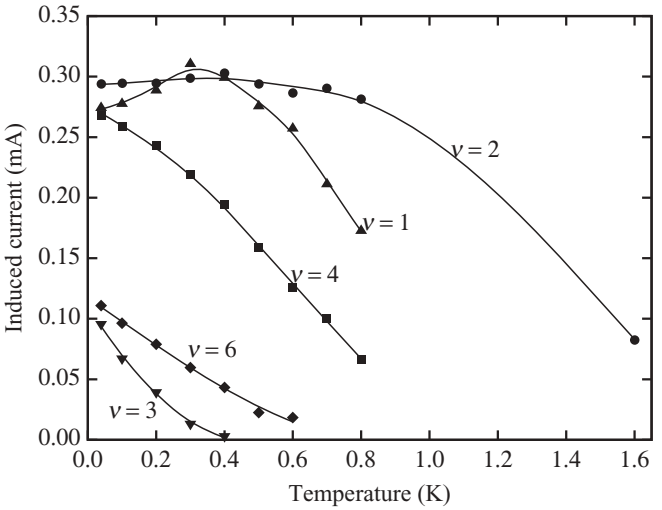

FIG. 4. Induced current amplitude vs temperature for $\nu =$ 1,2,3,4, and 6 at a sweep rate of 3.2 mT s^{-1}, corresponding to an electromotive force of 54 nV. The lines are guides to the eye.

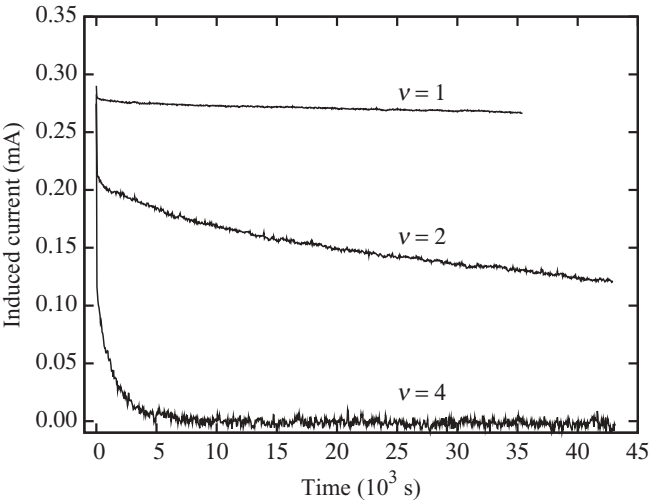

FIG. 6. Decay of the induced currents at $\nu = 1$,2, and 4, at 100 mK. Note that the x-axis zero has been offset to demonstrate that at the beginning of all three decays the current is 0.28 ± 0.02 mA.

TABLE I. Comparison of energy storage mechanisms for the induced current at $\nu = 4$, for a current of 0.29 mA.

Form of Storage	Calculated Value	Energy
Self-inductance of loop	3.1×10^{-8} H	1.29×10^{-15} J
Mutual inductance, loop + magnet		9.7×10^{-9} J
Capacitance	1.0×10^{-12} F	1.7×10^{-12} J

$E_\phi = 0$ and $E_r = Q/rC$. Hence, $dQ/dt = 2\pi r\sigma_{xx}Q/rC = Q/RC$ with the relaxation resistance R being given by $R = 1/2\pi\sigma_{xx}$. It is clear from this that Q decays exponentially with a time constant RC. The induced current has a current density associated with it given by

$$j_\phi = -\sigma_{xy}E_r + \sigma_{xx}E_\phi, \tag{6}$$

and so during the decay ($E_\phi = 0$) $j_\phi = -\sigma_{xy}E_r = -\sigma_{xy}Q/rC$. Consequently the induced current follows the same form of decay as Q.

B. The relationship of decays to *I*-*V* curves

As we have seen, the decay of induced currents involves dissipation of the capacitive energy through the resistance R, so we can write for the induced current

$$I = I_0 \exp(-t/RC). \tag{7}$$

The observation of slower than exponential decay implies that R is increasing with time, and hence that σ_{xx} is decreasing with time.

On the assumptions that $\sigma_{xx} \ll \sigma_{xy}$ and $j_r \ll j_\phi$ one can extract R from the I-V characteristic (which, in the terminology introduced above, is the dependence of I_ϕ on V_ϕ) as follows. The relaxation resistance R is V_r/I_r. From Eq. (5), $I_r = \sigma_{xy}V_\phi$; and from equation (6), $V_r = \alpha I_\phi/\sigma_{xy}$, where α is a geometric constant of order unity which depends on the radial distribution of I_ϕ. Thus $R = \alpha I_\phi/\sigma_{xy}^2 V_\phi$, or $V_\phi/I_\phi = \alpha/R\sigma_{xy}^2$; the nonlinearity of the I_ϕ-V_ϕ characteristic confirms that R increases with decreasing current, which also explains why it is increasing with time during a decay. Thus we can use the I-V characteristic to determine $R(I)$ and hence derive the shape of the decay curve (I vs t). There is a practical difficulty in doing this, which is that the discrete points of the I-V data need to be interpolated. In order to do this one must assume that the induced current at zero electromotive force is zero. To provide this interpolation we used a fit to the empirical function,

$$V = P_1 \sinh((P_2 I)^3), \tag{8}$$

where P_1 and P_2 are fitting parameters. This function is selected because it has the right symmetry properties, is smooth, and fits the I-V data within the noise, as shown in Fig. 2, for $\nu = 1$ at 800 mK (a), for $\nu = 2$ at 800 mK (b), and for $\nu = 4$ at 100 and 300 mK (c). We chose these filling factors and temperatures because the I-V curves show significant deviation from saturation at low electromotive force. The decay curves calculated from the I-V data are shown, along with the decay data, in Fig. 7. For $\nu = 1$ and 2, the calculated decay is similar to the measured decay, with small deviations caused by uncertainties in interpolation at low electromotive force. For the $\nu = 4$ decays, there is a systematic difference between the fit and the data, which is caused by the fact noted earlier that these decays exhibit an exponential dependence on time at large times. The empirical function of Eq. (8) was chosen to produce the time-varying R required to reproduce power-law decays; in contrast, an exponential decay requires constant R at large times. We have not been able to find an empirical function that fits the I-V data and reproduces both types of behavior at long times.

In order for this analysis to be useful, the data have to satisfy two conditions: (1) The I-V curve must include data at electromotive forces below the point at which the current saturates; and (2) the decay must be slow enough not to be significantly influenced by the transient behavior of the magnet when the sweep is stopped. All the data presented in Fig. 7 satisfy these conditions quite well. Data for other filling factors and temperatures presented in this paper do not, and are therefore excluded from this analysis: The I-V curves for $\nu = 1$ at 100 mK and for $\nu = 2$ at 100 and 300 mK (Fig. 2) do not satisfy condition (1); and the decays for $\nu = 6$, for $\nu = 4$ above 300 mK, and for $\nu = 2$ above 800 mK do not satisfy condition (2). Nevertheless the success of this analysis and its limitations are quite well demonstrated by the four data sets presented: The analysis is applicable in principle to all decays that show power-law dependencies at long times, i.e., for low filling factors and low to moderate temperatures. However, we have not been able to perform the analysis at the lowest temperatures because experimental limitations prevented us from achieving condition (1). The analysis does not work well for decays that show single exponential behavior at long times (large filling factors and high temperatures). In order to extend the applicability of this analysis we need to have a better understanding of the physical processes involved in the decay and I-V characteristics of induced currents, and their dependence on filling factor and temperature. This would enable us to replace the empirical function of Eq. (8) with one based on theory.

C. Temperature dependence

The temperature dependence of induced currents in the high-sweep-rate regime has been investigated previously by Matthews *et al.*[7] and interpreted in terms of the charge redistribution model of Kavokin *et al.*[8] Matthews *et al.* found that the low-temperature saturation current varied systematically with filling factor, whereas in the present sample it does not: The $\nu = 1$,2, and 4 data of Fig. 4 all show a low-temperature saturation current of 0.28 ± 0.02 mA (filling factors 3 and 6 are not observed to saturate). This leads us to propose that the saturation in this case is caused by electron self-heating (i.e., Joule heating), because this is the only mechanism we are aware of that does not depend on filling factor. It is not clear why our sample exhibits a filling-factor-independent saturation current while those studied previously show a systematic dependence of saturation current on filling factor. Following the discussion in the previous section, the power dissipated by the induced current, $I_r V_r = \alpha I_\phi V_\phi$, is of the order of 10^{-11} W. Based on the work of Price[19] and Wennberg *et al.*,[20] we can estimate the cooling power assuming that electrons cool by

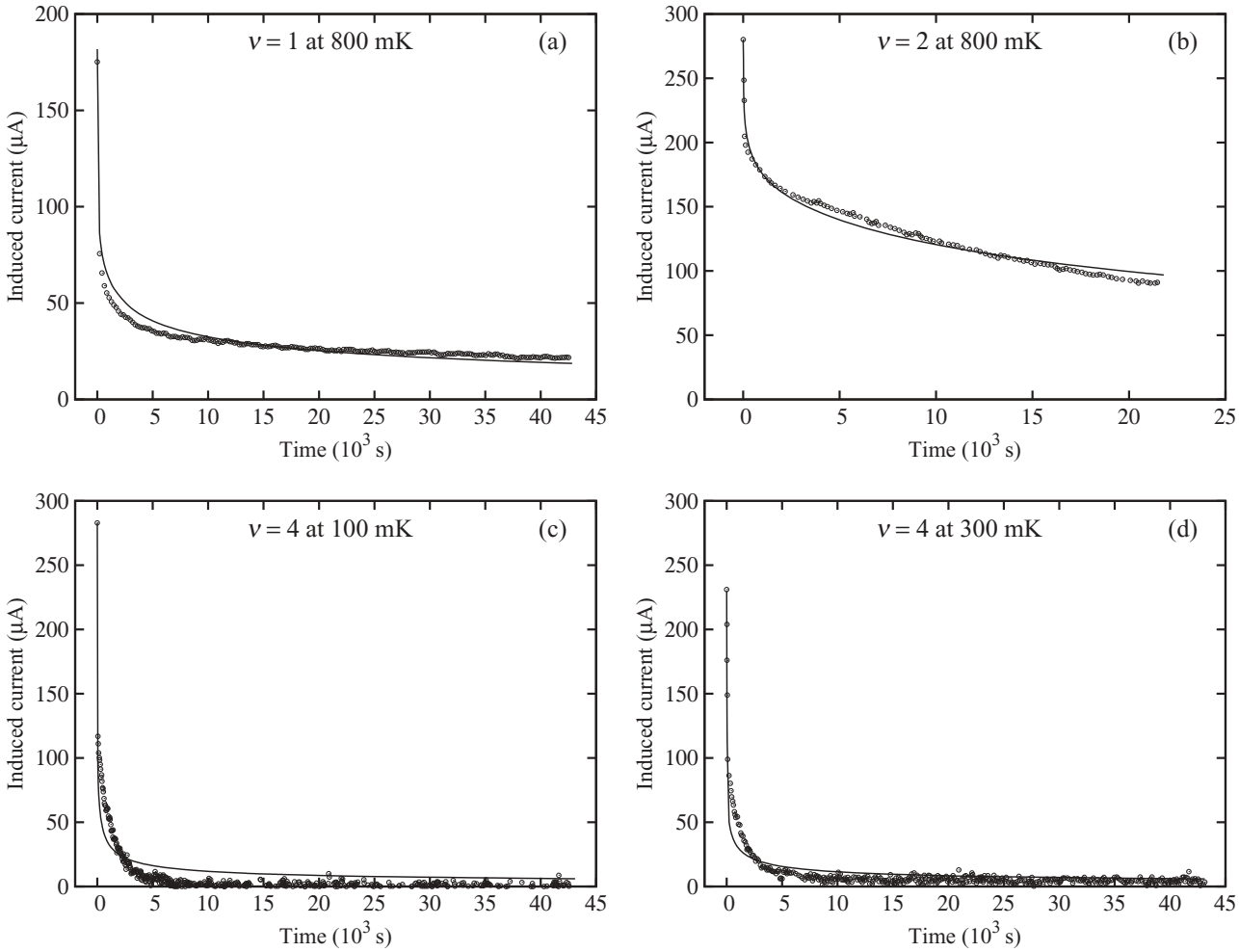

FIG. 7. Decay of the induced current (a) for $\nu = 1$ at 800 mK, (b) for $\nu = 2$ at 800 mK, (c) for $\nu = 4$ at 100 mK, and (d) for $\nu = 4$ at 300 mK. In each case the solid line is calculated from the corresponding sweep-rate I-V curve of Fig. 2 as described in Sec. IV B.

emitting phonons via a deformation potential interaction:

$$\text{Cooling power} \approx \frac{m^2 D^2}{w\rho\hbar^6 c^3 k_F}(k_B T)^4, \tag{9}$$

where m is the electron effective mass, D is the deformation potential,[21] w is the width of the 2DES, ρ is the mass density, c is the sound velocity, and k_F is the magnitude of the electron Fermi wave vector. The strong temperature dependence of the cooling power confirms that electron self-heating will become rapidly more important as the temperature is reduced. Equation (9) is only an approximation, but using reasonable values for its parameters we estimate that the cooling power becomes comparable with Joule heating at around 300 mK.

The other aspects of the filling-factor and temperature dependencies shown in Fig. 4 agree with the Kavokin model, in which the charge redistribution that accompanies induced currents leads to a shift in the quasi-Fermi energy towards an empty Landau level, which in turn increases the thermal activation rate of carriers into that level and hence increases the dissipation. This model predicts (a) that the saturation current of an I-V curve falls with temperature, exponentially in the highest quality 2DESs but approximately linearly in lower quality systems, and (b) that the temperature at which the saturation current drops to zero in lower quality systems (the intercept on the horizontal axis of Fig. 4) is proportional to the Landau-level separation at the Fermi energy. The fall with temperature is evident in all the data of Fig. 4, though the exact dependence varies with filling factor, suggesting that the quality of this 2DES is intermediate between the two limits discussed by Kavokin. The intercepts on the horizontal axis for even filling factors (1.7 ± 0.25 K for $\nu = 2$, 1.0 ± 0.05 K for $\nu = 4$, and 0.6 ± 0.1 K for $\nu = 6$) are approximately in the ratio of the energy gaps, $\hbar\omega_c$ ($\omega_c = eB/m^*$ and B is proportional to $1/\nu$); this ratio is $\frac{1}{2} : \frac{1}{4} : \frac{1}{6}$. Filling factors $\nu = 1$ and 3 have energy gaps equal to the Zeeman energy, $g^*\mu_B B$, which is smaller than $\hbar\omega_c$ for a given B. The $\nu = 1$ and 3 energy gaps should be in the ratio $1 : \frac{1}{3}$, which corresponds well with the ratio of their intercepts, 1.2 K to 0.4 K.

It is noteworthy that, while the data of Fig. 4 suggest that the $\nu = 1$ energy gap is smaller than that of $\nu = 2$ as expected from the argument above, the decays of Fig. 6 show that the $\nu = 1$ induced current has a slower decay than that at $\nu = 2$. To explain this we suggest that the decay process involves tunneling of electrons from full to vacant Landau levels, and that this tunneling process must conserve spin; as a result,

the separation between the levels involved in this tunneling is $\hbar\omega_c$ in both cases, and is therefore double the size at $\nu = 1$, compared with $\nu = 2$. In contrast, the process that reduces the saturation induced current at elevated temperatures, as seen in Fig. 4, is thermal excitation which involves phonons and can cause electrons to flip their spins, making the upper spin-split level accessible and resulting in an energy gap equal to the Zeeman splitting. Another mechanism that could flip electron spins is interaction with the nuclear spins of the host lattice. However, the spin relaxation mechanism is slow, and so one would expect it to have more effect on the slow decays of Fig. 6 than during the relatively fast sweeps associated with Fig. 4, the reverse of what we observe. While nuclear spin polarization could build up in our experiments giving rise to a considerable hyperfine field, the main effect of such a field would be an increase in Zeeman gap rather than enhanced relaxation rate. Nevertheless we cannot rule out the possibility that interaction with nuclear spin may play some role in the relaxation of induced currents.

V. CONCLUSIONS

Induced currents associated with the quantum Hall effect have been studied in the temperature range 39 mK to 1.6 K and at Landau-level filling factors $\nu = 1,2,3,4$, and 6 using torsion-balance magnetometry. Three energy storage mechanisms have been evaluated: capacitance, self-inductance, and mutual inductance. We have shown that the mutual inductance of the induced current in the superconducting magnet is the dominant mechanism for energy storage, and that the energy stored in this way is orders of magnitude larger than that stored via the capacitance or self-inductance mechanisms previously considered. We have shown that a single picture describes I-V and decay curves, and that the I-V curve can be used to predict the complex nonexponential decays observed for low filling factors and low to moderate temperatures. The temperature dependence of the saturation magnetic moment supports the Kavokin model[8] with the addition of a filling-factor-independent saturation current, limited by electron self-heating. A comparison of I-V curves and decays for $\nu = 1$ and $\nu = 2$ suggests that the dissipation process for the decay process at $\nu = 1$ conserves spin.

APPENDIX: ENERGY STORAGE IN INDUCED CURRENTS

1. Capacitive energy

$$\text{Capacitive energy} = \tfrac{1}{2} C V_r^2, \tag{A1}$$

where C is the capacitance of a loop around the edge of the sample. We can estimate this energy by estimating the capacitance, modeling the system as two parallel wires of separation d and radius w. The capacitance per unit length is then

$$C_l = \frac{\pi \epsilon_0 \epsilon_r}{\ln\left(\frac{d+(d^2-4w^2)^{1/2}}{2w}\right)}, \tag{A2}$$

provided that $d > 2w$. The logarithm in the denominator means that this capacitance is rather insensitive to assumptions about d and w. For instance if we assume that the separation between the charges is the radius of a circular sample having the area of the sample used in this experiment ($d = 2.4$ mm) and the "radius" of the charged regions is the magnetic length [$w = (\hbar/eB)^{1/2} = 1.76 \times 10^{-8}$ m] then $C = 4.8 \times 10^{-13}$ F. Alternatively if we make the (probably more realistic) assumption that the charge separation is governed by the edge-weighting of the Hall electric field[22] so that $d \sim 1$ μm, then $C = 1.6 \times 10^{-12}$ F. The value quoted in Table I, 1.7×10^{-12} J, is the average of these two estimates. V_r is obtained using Eq. (3) and a current of 0.29 mA.

The most extreme charge distribution that one could contemplate is the polarization of a circular sample into two regions of uniform charge density, the region from the center of the sample to a radius $1/\sqrt{2}$ times the sample radius containing a uniform excess of charge and the region outside this radius containing a uniform charge depletion. This distribution was used by Kavokin *et al.*[8] to explain the temperature dependence of the breakdown of the quantum Hall effect; the authors acknowledged that this distribution was extreme, but pointed out that the exact distribution used in their model did not affect its conclusions. Even using this distribution one obtains a capacitance and hence a stored energy only one order of magnitude larger than the value quoted in Table I.

2. Self-inductive energy

$$\text{Self-inductive energy} = \tfrac{1}{2} L_s I^2, \tag{A3}$$

where L_s is the self-inductance of the loop of length l around the sample perimeter and I is the induced current.

The self-inductance of a wire loop of radius d and cross-sectional radius w is

$$L_s = \mu_0 d \left[\ln\left(\frac{8d}{w}\right) - \frac{7}{4}\right]. \tag{A4}$$

Here we take d to be the radius of a circular sample of equivalent area ($d = 2.4$ mm). The value of L_s and hence the self-inductive energy is only weakly dependent on the assumed value of w; if w is taken to be the magnetic length, one obtains a self-inductive energy of 1.54×10^{-15} J; taking w to be the width of the region at the edge of the sample having significant Hall electric field, ~ 1 μm, gives 1.03×10^{-15} J. The average of these estimates is quoted in Table I.

3. Mutual-inductive energy

$$\text{Mutual-inductive energy} = M I_m I, \tag{A5}$$

where I_m is the current in the solenoid, and M is the mutual inductance given by $M = k\sqrt{L_m L_s}$, L_m being the self-inductance of the magnet solenoid and $-1 \leqslant k \leqslant 1$ is a coupling coefficient.

To estimate the energy stored in this mutual inductance we note that this energy is simply the energy $mB\cos\theta$ that would be required to bring the sample, having magnetic moment m, from infinity into the magnetic field B corresponding to $\nu = 4$ (2.5 T). The result is a mutual-inductive energy of 9.7×10^{-9} J. Note that we did not need to estimate the mutual inductance from the experimental setup in order to obtain this energy.

[1] A. Usher and M. Elliott, J. Phys.: Condens. Matter **21**, 103202 (2009).
[2] J. P. Eisenstein, Appl. Phys. Lett. **46**, 695 (1985).
[3] T. Haavasoja, H. L. Störmer, D. J. Bishop, V. Narayanamurti, A. C. Gossard, and W. Wiegmann, Surf. Sci. **142**, 294 (1984).
[4] C. L. Jones, A. Usher, M. Elliott, W. G. Herrenden-Harker, A. Potts, R. Shepherd, T. S. Cheng, and C. T. Foxon, Solid State Commun. **97**, 763 (1996).
[5] J. P. Watts, A. Usher, A. J. Matthews, M. Zhu, M. Elliott, W. G. Herrenden-Harker, P. R. Morris, M. Y. Simmons, and D. A. Ritchie, Phys. Rev. Lett. **81**, 4220 (1998).
[6] A. J. Matthews, J. P. Watts, M. Zhu, A. Usher, M. Elliott, W. G. Herrenden-Harker, P. R. Morris, M. Y. Simmons, and D. A. Ritchie, Physica E **6**, 140 (2000).
[7] A. J. Matthews, K. V. Kavokin, A. Usher, M. E. Portnoi, M. Zhu, J. D. Gething, M. Elliott, W. G. Herrenden-Harker, K. Phillips, D. A. Ritchie, M. Y. Simmons, C. B. Sorensen, O. P. Hansen, O. A. Mironov, M. Myronov, D. R. Leadley, and M. Henini, Phys. Rev. B **70**, 075317 (2004).
[8] K. V. Kavokin, M. E. Portnoi, A. J. Matthews, A. Usher, J. Gething, D. A. Ritchie, and M. Y. Simmons, Solid State Commun. **134**, 257 (2005).
[9] J. D. Gething, A. J. Matthews, A. Usher, M. E. Portnoi, K. V. Kavokin, and M. Henini, Int. J. Mod. Phys. B **18**, 3537 (2004).
[10] C. L. Jones, A. Usher, M. Elliott, W. G. Herrenden-Harker, A. Potts, R. Shepherd, T. S. Cheng, and C. T. Foxon, Solid State Commun. **95**, 409 (1995).
[11] T. Klaffs, V. A. Krupenin, J. Weis, and F. J. Ahlers, Physica E **22**, 737 (2004).
[12] J. Huels, J. Weis, J. Smet, K. von Klitzing, and Z. R. Wasilewski, Phys. Rev. B **69**, 085319 (2004).
[13] M. Pioro-Ladrière, A. Usher, A. S. Sachrajda, M. Elliott, J. Lapointe, J. Gupta, Z. R. Wasilewski, and S. Studenikin, Physica E **34**, 476 (2006).
[14] M. Pioro-Ladrière, A. Usher, A. S. Sachrajda, J. Lapointe, J. Gupta, Z. Wasilewski, S. Studenikin, and M. Elliott, Phys. Rev. B **73**, 075309 (2006).
[15] T. J. Kershaw, A. Usher, A. S. Sachrajda, J. Gupta, Z. R. Wasilewski, M. Elliott, D. A. Ritchie, and M. Y. Simmons, New J. Phys. **9**, 71 (2007).
[16] D. B. Chklovskii, B. I. Shklovskii, and L. I. Glazman, Phys. Rev. B **46**, 4026 (1992).
[17] Institute for Microstructural Sciences, NRC-CNRC Canada, sample designation "AK47."
[18] A. J. Matthews, A. Usher, and C. D. H. Williams, Rev. Sci. Instrum. **75**, 2672 (2004).
[19] P. J. Price, J. Appl. Phys. **82**, 6863 (1982).
[20] A. K. M. Wennberg, S. N. Ytterboe, C. M. Gould, H. M. Bozler, J. Klem, and H. Morkoç, Phys. Rev. B **34**, 4409 (1986).
[21] *Crystal and Solid State Physics, Semiconductors*, edited by O. Madelung, M. Schulz, and H. Weiss, Landolt-Börnstein, New Series, Group III, Vol. 17 (Springer-Verlag, Berlin, 1982), Sec. 2.10.1, p. 224.
[22] A. H. MacDonald, T. M. Rice, and W. F. Brinkman, Phys. Rev. B **28**, 3648 (1983).